Available online at www.sciencedirect.com
ScienceDirect
Journal of the European Ceramic Society 29 (2009) 2369–2378
www.elsevier.com/locate/jeurceramsoc

Mechanical and fatigue strengths of silicon nitride ceramics in liquid aluminum alloys

Mitsuhiro Okayasu [a,*], Masuo Hitomi [b], Hirotsugu Yamazaki [b]

[a] *Department of Machine Intelligence and Systems Engineering, Akita Prefectural University, 84-4 Ebinokuchi, Tuchiya-aza, Yurihonjo-city, Akita, 015-0055, Japan*
[b] *Yamazaki Diecast Corporation Limited, 59 Aza-Kawahara Nakano Misto-cho, Akita, 019-1521, Japan*

Received 9 October 2008; received in revised form 29 December 2008; accepted 13 January 2009
Available online 10 February 2009

Abstract

Although the silicon nitride ceramic (Si_3N_4) has a high mechanical strength even at high air temperature, much reduction in the material strength occurs in liquid aluminum alloys. The bending strength of the ceramic in molten Al alloys is about 20% lower than that obtained in an air temperature of 750 °C. Moreover, a significant reduction of the fatigue strength occurs in the Al alloy melt. The change of mechanical properties of Si_3N_4 ceramic in the melt also depends on the amount of iron in the molten aluminum alloy; a large amount of iron makes the fatigue strength low. The reduction in the material strength is attributed to the change of material properties caused by the chemical reaction between iron and silicon nitride. Details of the chemical reaction in Si_3N_4 ceramic are discussed in the present work.

Keywords: Si_3N_4 ceramic; Aluminum alloy; Diffusion; Fatigue property; Material property

1. Introduction

Silicon nitride ceramics possess good material properties, including high strength, oxidation resistance and low thermal expansion coefficient. Good material properties for the ceramic are also maintained even at high temperature in the atmosphere, so have been used for various structures and components. Specifically, stringent demands on material strength for various structures and components have been met by the use of silicon nitride ceramics, e.g., Si_3N_4. For the applications of the ceramic, the fundamental study of the material properties of Si_3N_4 was performed by many researchers, and the useful experimental data have been obtained.[1–11] Mechanical seals protect the environment from product leakage in various equipments, including engines and turbines, with rotating shafts or alternative moment parts. It appeared from the recent studies that a high extent dynamic sealing (or wear) of Si_3N_4 is obtained as sealed with a grey cast iron rings[1] compared with the silicon nitride/silicon carbide rings, because of the protection by a tribolayer composed of amorphous silica and ferrous oxide. The examination of the chemical stability of Si_3N_4 cutting tools in the machining of Fe-based alloys has also been conducted, and it was found that the chemical reaction occurred in the ceramic side, and the reinforcement phases of high chemical stability contributed to increase the chemical/diffusive wear resistance.[2,3]

Recently, the use of the Si_3N_4 ceramic for the shot-sleeve in die-casting technology has received special attention.[12,13] Ceramic shot-sleeves have replaced those made from hardened carbon steels. Die-casting technology is one of the most widely employed manufacturing processes for producing various automotive parts, such as transmission cases and cylinder blocks. The advantage of the die-casting process is high productivity and the ability to cast components with thin walls and complicated geometries.[14,15] There are several reasons for replacing steel sleeves by ceramic ones: (i) they require less lubricant between the shot-sleeve and plunger[12]; (ii) they have a low coefficient of thermal conductivity and (iii) excellent high temperature strength. In addition, high quality die-casting components can be created by using a ceramic sleeve, with fewer internal defects and better mechanical properties. Although the ceramic injection system has several advantages,[16,17] ceramic sleeves have seldom been used in die-casting processes, especially for alu-

* Corresponding author.
E-mail address: okayasu@akita-pu.ac.jp (M. Okayasu).

0955-2219/$ – see front matter © 2009 Elsevier Ltd. All rights reserved.
doi:10.1016/j.jeurceramsoc.2009.01.013

minum alloy. In our previous work, an attempt was made to use a ceramic sleeve in Al alloy hot-chamber die-casting. In this die-casting process, higher quality components were produced compared to those from the steel injection system, for instance, the tensile strength of Al alloy produced by the ceramic sleeve is about 1.3 times higher than that for the steel system.[18] However, since the ceramic sleeve is immersed in molten aluminum alloys for long periods of time, corrosion and abrasion arise on the ceramic surface. Furthermore, the ceramic sleeve sometimes fractures into several pieces during the die-casting process. For this reason, the die-casting production has to stop to change the ceramic sleeve every 2 or 3 weeks, and this delay results in a reduction of the use of ceramic sleeves in the die-casting industry. Because it is known that Si_3N_4 ceramic has high strength even at high air temperature, the material properties must be subjected to alteration in the molten aluminum alloy. In order to use ceramic sleeves in the Al alloy die-casting process, an examination of the fundamental aspects of the material properties of the ceramic in molten Al alloys is required. This information is particularly significant in the design of shot-sleeves. The aim of

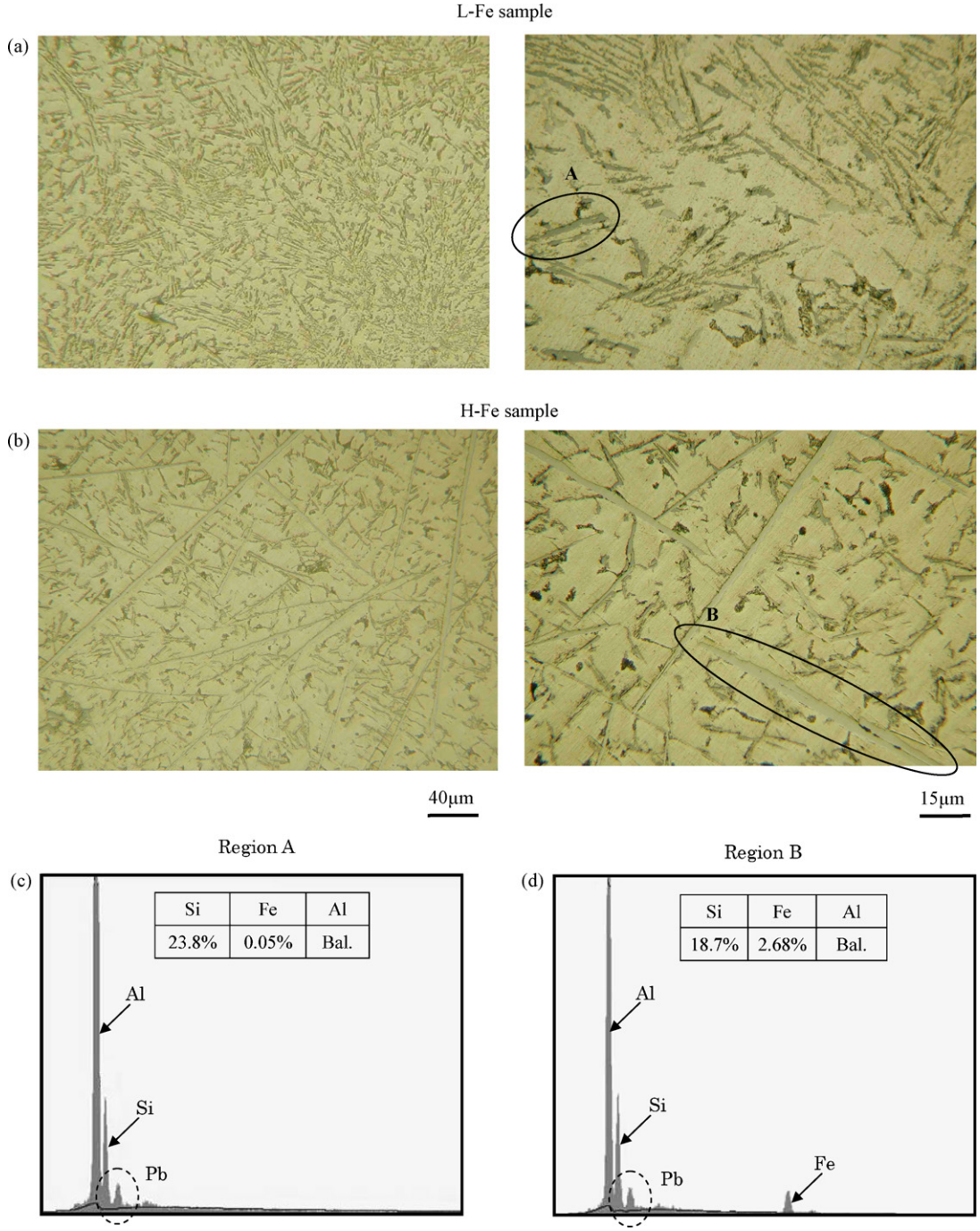

Fig. 1. Optical micrographs of the Al–Si–Cu alloy with different iron contents: (a) 0.7%Fe and (b) 1.7%Fe. (c) and (d) EDX analysis of the 2nd phase in regions A and B of (a) and (b), respectively.

this work was, therefore, to investigate the fatigue and bending strengths of Si_3N_4 ceramics in liquid Al alloys, and to compare their strengths with those obtained at various air temperatures.

2. Experimental procedures

2.1. Materials and test conditions

The specimens used in the present work were from a commercial Si_3N_4 ceramic, fabricated by sintering α-Si_3N_4 powder with sintering aids. The chemical composition was estimated to be (in wt.%): 54 Si, 37 N, 4 Y, 3 Al and 2 O. The Si_3N_4 ceramic employed was the same material as the actual ceramic shot-sleeve for the die-casting system. In the examination of the mechanical properties, specimens were machined into rectangular bars 2 mm × 2 mm × 50 mm. The mechanical properties were investigated by three-point bending tests under various conditions: (i) at room temperature (298 K); (ii) at high air temperatures (573 K and 1023 K); and (iii) in the molten aluminum alloy (973 K). In the last test, die-casting aluminum alloys, having either a low amount of iron 0.7% (L-Fe) or a high amount of iron 1.7% (H-Fe), were used. Both aluminum alloys were made based upon ADC10 (wt.%): 8.6 Si, 3.4 Cu, 0.17 Mg, 0.7 or 1.7 Fe and balanced with Al. The microstructures of the aluminum alloys and their EDX analysis are shown in Fig. 1. By comparing those microstructures, short (region A) and very long (region B) needle shaped particles of a 2nd phase can be observed in the L-Fe and H-Fe samples, respectively. As can be seen in the X-ray spectrum (Fig. 1(d)), characteristic peaks for Fe, Si and Al are detected above a continuous X-ray background in the long needle-like 2nd phase (region B). Its composition is considered to be Al_5FeSi.[19] On the other hand, the short fiber-like phase could be related to eutectic Si (region A),[20] Fig. 1(c). It should be noted that the peak for Pb, enclosed with the dashed line in both X-ray spectra, derives from the metal deposited on the surface of the sample for the EDX analysis.

The bending and fatigue strengths of the Si_3N_4 ceramic were investigated using a screw driven type universal testing machine with 1 ton capacity. A muffle furnace with an accuracy of better than 0.1 K was fitted into this testing machine, and used for the high temperature tests. The static bending test and low-cycle fatigue test were carried out at a speed of 1 mm/min. The fatigue cycle is illustrated in detail in Fig. 2, and was designed on the basis of a die-casting shot cycle, with cycle time 15 s. The

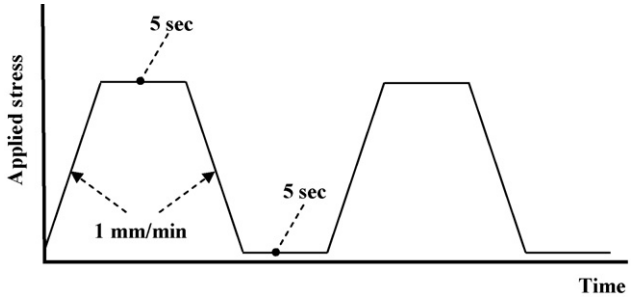

Fig. 2. Schematic illustration of the fatigue cycle.

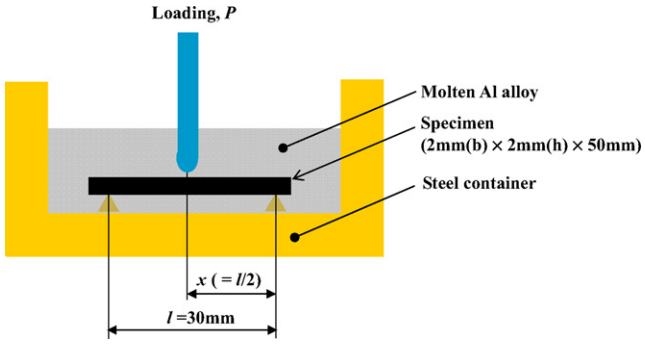

Fig. 3. Schematic illustration showing experimental setup for the fatigue and bending tests in the molten aluminum alloys.

stress amplitude in this test is determined from the following expression:

$$\sigma_{max} = \frac{3lP_{max}}{2bh^2} \quad (1)$$

where l is the loading span, P_{max} is the maximum applied load, and b and h are the specimen width and height, respectively. The maximum cyclic load, P_{max}, was chosen based upon the average bending strength (P_f) of the Si_3N_4 ceramic, e.g., P_{max} is less than 90% of the P_f value. To obtain the mechanical properties of samples in the molten Al alloys, the bending tests were executed while immersed in the liquid aluminum alloy filling a small container, made of the medium carbon steel (in wt.%): 0.45 C, 0.2 Si, 0.75 Mn and balanced with Fe (Fig. 3). The Al alloy was melted and heated to 973 K in the muffle furnace.

3. Results and discussion

3.1. Bending properties of Si_3N_4 ceramic

Table 1 indicates the average bending strength obtained under various conditions, namely in the atmosphere at 298 K, 573 K and 1023 K and in the molten Al alloy. Fig. 4 shows the representative stress–deflection curves. Note that in the molten Al alloy test, the aluminum alloy with 0.7%Fe (L-Fe) was employed. The experimental results show that the bending strength depends on the test conditions. The bending strengths for the sample tested at room temperature and at 573 K are almost the same, but this decreases slightly as the sample is heated to 1023 K. A considerable drop in the strength was obtained when the sample was immersed in the liquid aluminum alloys. The mechanical properties of the sample in the melt are further examined in the next section. It should be pointed out that the overall slope of the stress–deflection (S–D) curve is similarly observed for all the

Table 1
Bending strength of the samples tested in various conditions.

	Bending strength
298 K	980 ± 35 MPa
573 K	975 ± 35 MPa
1023 K	872 ± 35 MPa
In molten Al alloy (973 K)	737 ± 60 MPa

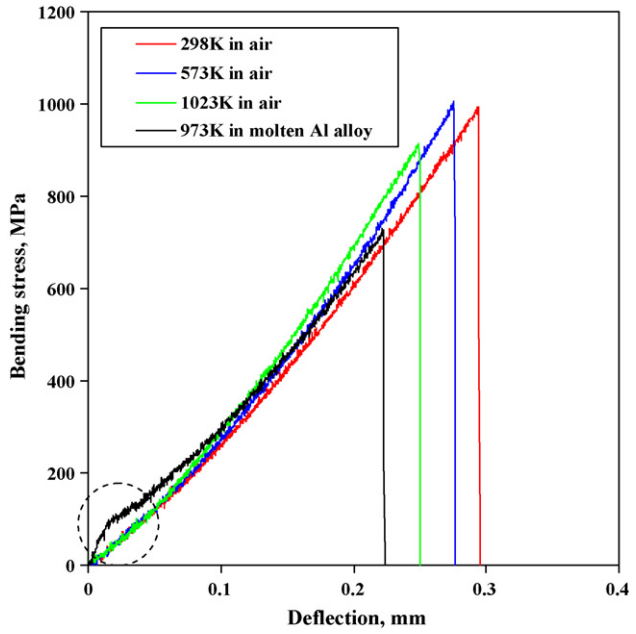

Fig. 4. Bending stress vs. deflection relationships for the Si_3N_4 ceramics tested under various conditions.

samples (about 300 MPa/mm) although the bending strength is altered. In this case, the different strength would be related to the change of the material properties when heated in air and in liquid Al alloy. However, it cannot be considered the material softness occurred even in the high temperature conditions because of the similar slope of S–D curve. Details of the material properties at the high temperatures will be discussed below.

To understand the reasons for the slight reduction in the bending strength at 1023 K in air, the material properties were investigated by TG and DTA. The TG and DTA curves were obtained using a heating rate of 20 K/min from room temperature to 1273 K. The sample, crushed into small pieces, was treated thermally in a TG–DTA measurement instrument in air. Fig. 5 exhibits the variation of the TG and DTA data as a function of the sample temperature. In this measurement the data were taken directly from the digital output provided by the thermobalance. The DTA data shows a large endothermic reduction above 700 K, which is similarly seen in the previous work.[21] The small mass change taking place in the beginning of the heating stage below 950 K might be due to the loss of water or the remnants of volatile impurities. On the other hand, the Si_3N_4 weight increases above 950 K,[22] which would be influenced by the oxidation of Si_3N_4.[21] In this case, the oxidation of Si_3N_4 ceramic could occur with different extent, depending on the air temperature.[23] In the previous work, it is reported that, at the low temperature, e.g., below 1283 K, the oxidation effects detect preferentially located at concentrations of the intergranular phase even though a very thin amorphous silica film is formed on exposed silicon nitride grains. The oxidation of Si_3N_4 ceramic contains an assumption that the ceramic forms silicon dioxide and nitrogen when heated in air in accordance with the reaction:

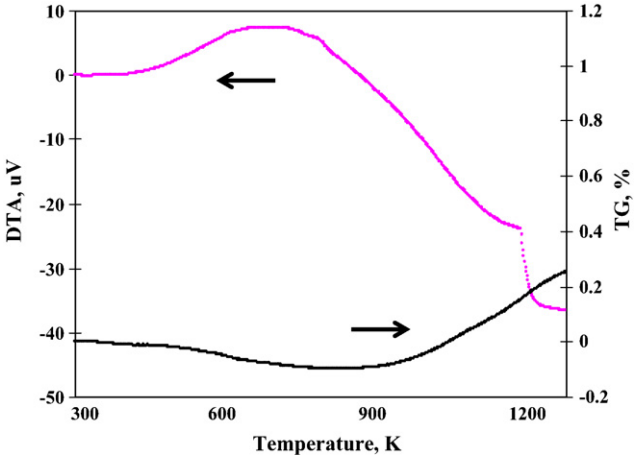

Fig. 5. TG and DTA curves for the Si_3N_4 ceramic as a function of sample temperature.

$$Si_3N_4 + 3O_2 \rightarrow 3SiO_2 + 2N_2 \quad (2)$$

This chemical reaction is one of the first assumptions.[22] The other possible products are silicon dioxide, silicon oxynitride Si_2ON_2 and nitrogen oxide (N_2O, NO, NO_2); the probable reactions are

$$Si_3N_4 + 5O_2 \rightarrow 3SiO_2 + 4NO \quad (3)$$

$$Si_3N_4 + 3SiO_2 \rightarrow 6SiO(gas) + 2N_2 \quad (4)$$

On the basis of the above reactions, it is considered that the reduction/oxidation in the silicon nitride could occur during the heating process. In addition, from the above chemical reactions, the oxygen and nitrogen defects could be generated in the Si_3N_4 ceramic. It is reported that the atom vacancy, e.g., oxygen, nitrogen and silicon, can occur in Si_3N_4 ceramic. The silicon vacancy (V_{si}) in the ceramic is created when oxygen atoms are incorporated into the Si_3N_4 crystal lattice and substitute onto a portion of the nitrogen site:[24]

$$2O_2 \rightarrow 4O_N + V_{si} \quad (5)$$

The crystal phases in the silicon nitride ceramic can change when heated above 1023 K, where the crystalline phase of α- and β-Si_3N_4 alters.[24] The occurrence of atom vacancy is reflected to the change of the material color. To substantiate whether or not the atom vacancy occurs in our silicon nitride, a direct observation was carried out. Optical macrographs of the sample heated to about 1023 K and that at room temperature are displayed in Fig. 6. As can be seen, the surface of the high temperature sample is whitened compared to the room temperature one. From the change of the surface status, it may be considered that the atom vacancy in the silicon nitride is created.[25] Yuan et al.[26] reported that the reduction in mechanical properties of the ceramic occurs at high air temperature because of the presence and diffusion of internal defects.[27,28] Those are the possible reasons to induce the reduction in the bending strength of our ceramics at the high air temperature in Table 1 and Fig. 4.

It is interesting to mention that the stress–deflection curve in the beginning of the loading process (Fig. 4) shows convex profiles for the samples tested in the molten Al alloys, while the others have concave profiles, as shown with the dashed

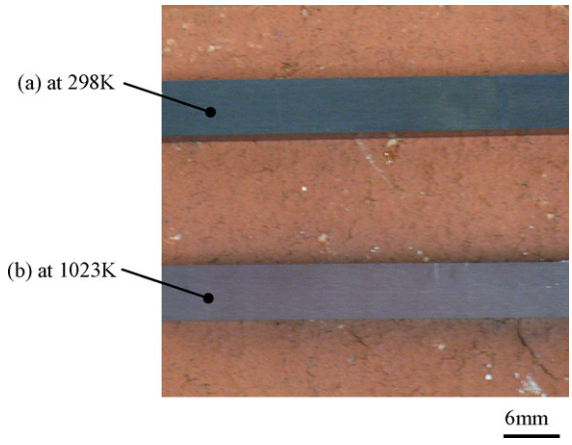

Fig. 6. Optical macrographs of the Si_3N_4 ceramic: (a) at room temperature and (b) at the high air temperature (1023 K).

circle. The existence of a concave stress–deflection relation is observed in many engineering materials.[29] On the other hand, in the study by Pushpalal,[30] a convex stress vs. deflection relation was obtained, for a three-point bend test conducted using an aluminate–phenol resin composite material. The reason for this is affected directly by the different material property, e.g., viscoelastic behavior. From his work, the convex stress vs. deflection obtained in Fig. 4 might also be influenced by the change of the material property during the immersion in the molten Al alloy. This will be further discussed in a later section of this report.

3.2. Fatigue properties

The fatigue behaviors for the Si_3N_4 ceramics tested at 298 K and in the two different molten aluminum alloys (L-Fe and H-Fe) are shown in Fig. 7. In a similar way to a conventional S–N relationship, the number of cycles to failure increased in both cases with decrease of the maximum applied stress. For the sample tested in the atmosphere, the mean endurance limit (σ_l) at 10^5 cycles is about 760 MPa, which is a similar value to the related silicon nitride ceramic.[31] The fatigue limit at room temperature is more than 1.3 times higher than that in the molten aluminum alloys. By comparing L-Fe vs. H-Fe aluminum alloy, the fatigue strength in the L-Fe melt is found to be about 1.4 times greater than that for H-Fe. In the study of Qiao et al.,[32] the fatigue strengths of Si_3N_4 ceramics were investigated in various conditions, in air (room temperature), in water and in kerosene, and they found that the fatigue strength in water is lower than that for the air test sample. Their experimental results implied that the test environment is sensitive to the mechanical properties of the Si_3N_4 ceramic.

To understand the fatigue behavior of this ceramic, the stress vs. deflection relationship was examined. Fig. 8(a) and (b) shows the stress–deflection curves obtained at several stages during the fatigue test in the liquid Al alloys and in the atmosphere at 298 K, respectively. It should be pointed out that the numbers, 944 cycles and 250 cycles, indicated in Fig. 8(a) and (b), show the fatigue cycle number just before the final failure of the specimen. It is seen that different trends of stress vs. deflection are

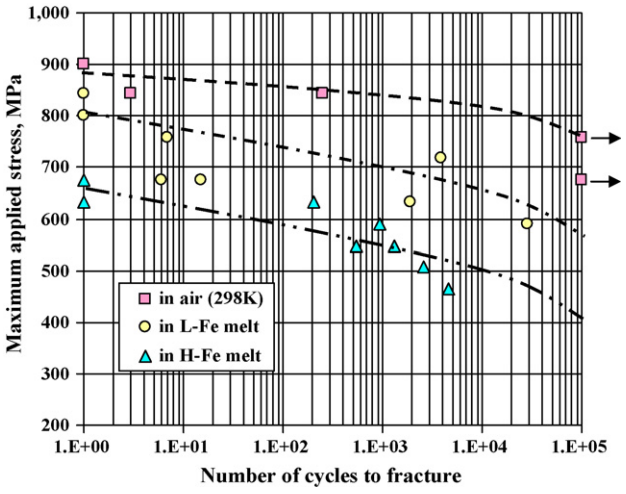

Fig. 7. Maximum stress vs. number of cycles to failure for the Si_3N_4 ceramic.

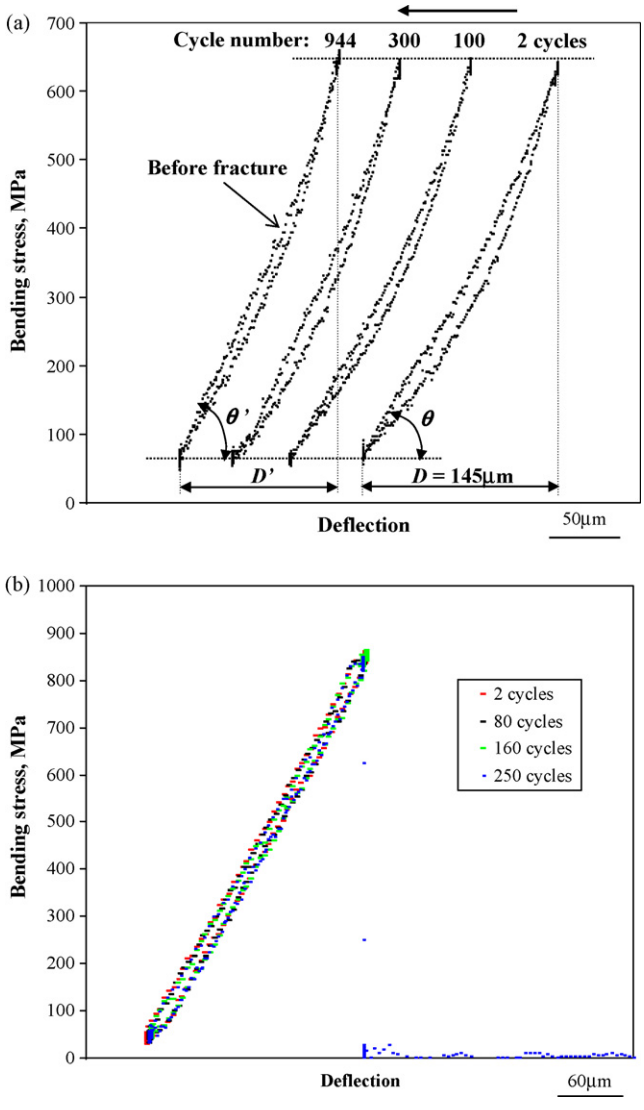

Fig. 8. Bending stress vs. deflection of the Si_3N_4 ceramic tested at several stages: (a) in the molten Al alloy and (b) in atmosphere (298 K).

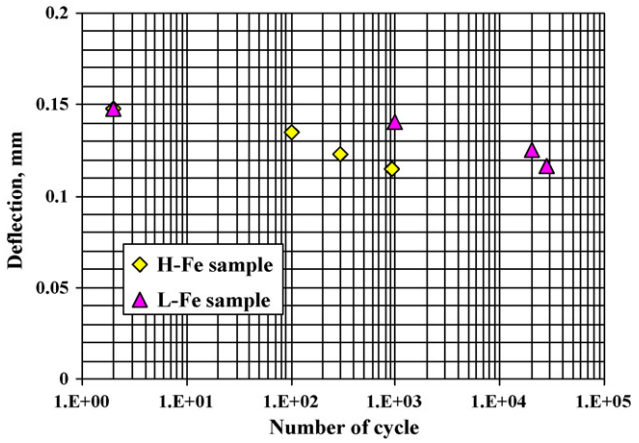

Fig. 9. Variation of the deflection value during cyclic loading for the Si_3N_4 ceramic tested in the molten Al alloy with 0.7%Fe (L-Fe) and 1.7%Fe (H-Fe).

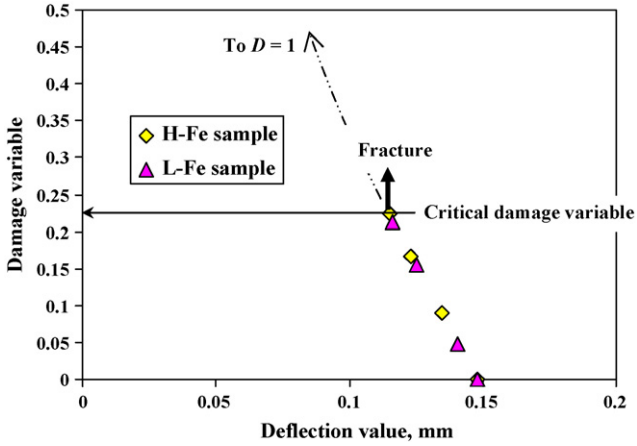

Fig. 10. Damage variable vs. deflection value for the samples tested in the molten Al alloys.

obtained in the molten Al alloy, and this depends on the specimen status, including, for instance, the deflection value (D) and the slope of the loading stage (θ). It is obvious that the deflection value decreases (or slope of θ increases) with increasing cycle number, which might be attributed to a change of material property. In contrast, no clear change of stress–deflection curve is obtained till the final fracture in the atmosphere test, as shown in Fig. 8(b). It could be considered from the results that the material properties change significantly in the Al alloy melt. To understand the change of material properties, the variation of the deflection value during the cyclic loading was examined at several stages. Fig. 9 presents the deflection value vs. cycle number for the samples loaded cyclically at σ_{max} 675 MPa in the L-Fe and H-Fe melts. As can be seen, both deflection values in the beginning of the fatigue test have the same value, approximately 0.145 mm, and that this value decreases with increasing cycle number, but at a different rate. The deflection falls faster for the H-Fe sample than for the L-Fe sample. An important observation from Fig. 9 is that both samples are fractured as the deflection level reaches about 0.115 mm. Because the deflection value decreases by about 20% during the cyclic loading, the test samples must have been hardened in the molten aluminum alloy. In addition, due to the different reduction rate between the L-Fe and H-Fe samples, the amount of iron may affect the change of material properties in the Si_3N_4 ceramic.

The value of the deflection was verified numerically using a model of a supported beam of span l with a concentrated load P at its mid-span, as shown in Fig. 3. In this model, the deflection value can be estimated by the following formula[33]:

$$v = \frac{Pl^3}{48EI} \tag{6}$$

where EI is the flexural rigidity of the beam. As shown in Fig. 3, $l = 30$ mm and $b = h = 2.0$ mm, and the elastic constant of the Si_3N_4 ceramic is $E = 300$ GPa.[34] In this experiment, the applied load, P, was defined as the maximum cyclic load of 120 N. From Eq. (6), the calculated deflection value is $v = 0.17$ mm, and this value is relatively close to the experimentally obtained data, e.g., the deflection at the beginning of fatigue test, $v = 0.145$ mm, as seen in Fig. 9.

In Fig. 9, the deflection value in the ceramic changed during the fatigue process, and the material properties would have been altered due to the material damage. There are various factors that contribute to an understanding of the material damage, e.g., elastic modulus, density and hardness.[35] Considering the damage factors, an attempt was made to interpret the variation of material damage in our sample. In this approach, the deflection of the specimen was used as a damage variable factor (D), since that deflection value is altered during the fatigue test as described above. The deflection value and damage variable can be expressed as follows:

$$v = \frac{Pl^3}{48EI(1 - D)} \tag{7}$$

$$D = 1 - \frac{\tilde{v}}{v} \tag{8}$$

where $\tilde{v}$ is the initial deflection level.[35] Using the damage variable, the value of the critical damage at the sample fracture point can be determined. The D values, calculated using the experimental data in Fig. 9, are plotted in Fig. 10. As can be seen, the damage variable increases with decrease of the deflection level in both L-Fe and H-Fe samples. It is also found from Fig. 10 that as the damage variable reaches 0.23, an unstable fracture occurs in this ceramic.

An examination of the material properties after immersion in the L-Fe and H-Fe samples was carried out. Fig. 11(a) and (b) depicts the optical macrograph and SEM image of the specimens (H-Fe and L-Fe) after immersion in the liquid Al alloys for 24 h. As can be seen, the aluminum alloy was stuck to the specimen surfaces, and could not be scraped off easily. A large area of Al alloy is observed on the H-Fe sample, showing where the molten metal would be strongly bonded to the ceramic surface in Fig. 11(b). Such metal bonding might be attributed to a chemical reaction. The large area of Al alloy on the H-Fe sample may be associated with a stronger chemical reaction involving iron in the Al alloys.

To verify this, the material properties of the Al alloy on the Si_3N_4 ceramic surface were examined by EDX analysis. Fig. 12 represents the EDX analysis of the Al alloy bonded on to the

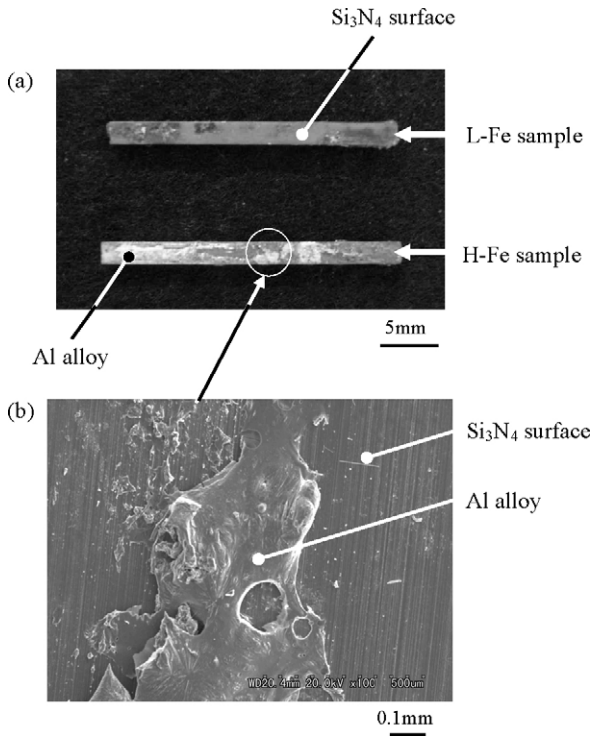

Fig. 11. (a) Optical macrograph of Si_3N_4 after immersion in the molten Al alloy (H-Fe) for 24 h showing the aluminum alloy on the ceramic. (b) SEM image of the Si_3N_4 ceramic.

Si_3N_4 ceramic (H-Fe sample Fig. 11). This analysis was performed on an area 10 μm × 10 μm and shows intense peaks of Al and Si as well as a clear weaker peak of Fe (2.33%). As the iron content is 1.7% in the H-Fe aluminum alloy as described in the previous section, the Fe element appears to be concentrated

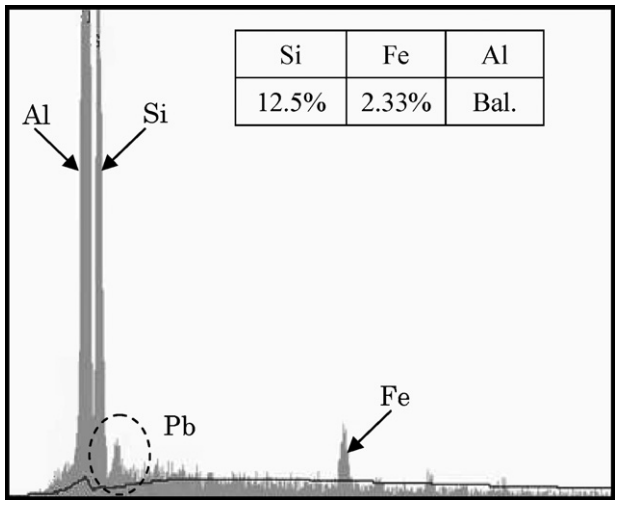

Fig. 12. EDX analysis obtained from the Al alloy on the Si_3N_4 ceramic in Fig. 11.

adjacent to the Si_3N_4 ceramic. To confirm this, measurements of the SEM image and an EDX analysis were performed. Fig. 13 shows the SEM image of the fracture surface of the ceramics, and the EDX mapping obtained from the same area of the SEM image. Note the sample for this observation was fractured after immersion in the molten aluminum alloy (H-Fe) for 24 h. As can be seen in Fig. 13(c), there is aluminum around the ceramic, related to the attached Al alloy, as shown in Fig. 11. Interestingly, iron can also be clearly detected in some specific areas surrounding the Si_3N_4 ceramic as indicated by the arrows in Fig. 13(d). In this case, the iron atoms would have diffused to the Si_3N_4 ceramic. Oliveira et al. have examined the contact characteristic between silicon nitride ceramics and steels.[6] With their observation of the interface between Si_3N_4 ceramic and medium carbon

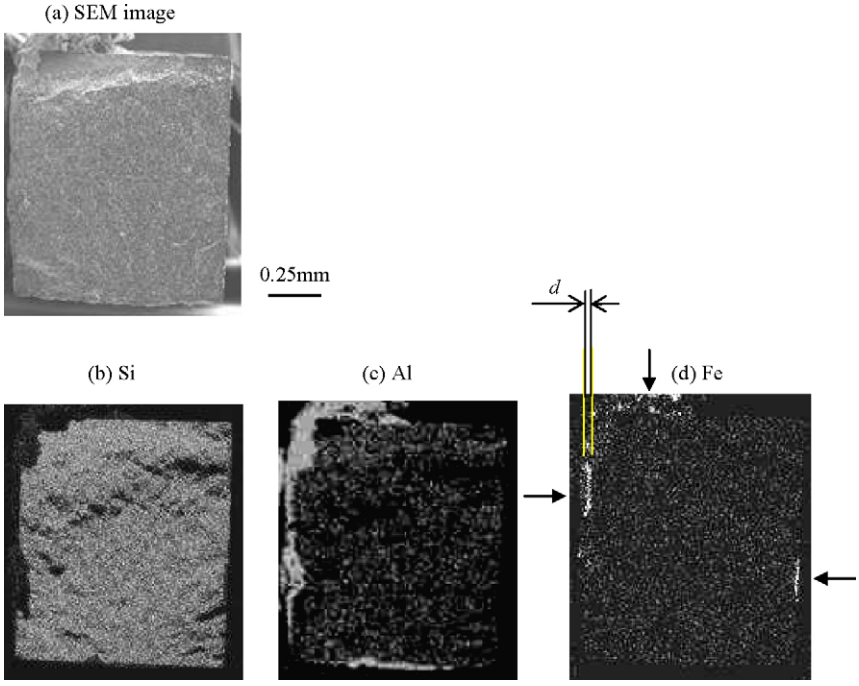

Fig. 13. EDX analysis of the fracture surface of the Si_3N_4 ceramic and the Al alloy around the ceramic taken by scanning for Si, Al and Fe.

steel (AISI 1045), it appeared there are two different chemical reaction zones, e.g., the consumed ceramic zone and the diffusion zone. The diffusion area corresponds to the $\alpha/(\gamma+\alpha)$-Fe phase boundary with a net shift of the Si and C concentration, and the formula to compute the thickness of the reaction zone can be proposed.[6]

$$r^2 = 2K_r(t - t_0) \tag{9}$$

where r is the thickness of consumed ceramic, K_r is the parabolic reaction constant, t is the time and t_0 is the induction time of the reaction. With Eq. (9), the estimation of the r value for our sample can be performed, where K_r is 18.1×10^{-16} m^2/s and t_0 is taken as 1.8 h. As the testing time t is 24 h, r^2 becomes a constant, i.e., $r^2 = 2K_r(t - t_0) = 289.3$ μm^2 according to Eq. (9). Using the r value, the diffusion zone thickness (d) can be further estimated[6]:

$$d - d_0 = br \tag{10}$$

where b and d_0 are the material constants, and $b = 8.3$ and $d_0 = 12.9$ μm for Fe.[6,36] If the value of r is about 17.0 μm from Eq. (9), the d value can be approximated as 154.1 μm according to Eq. (10). As shown in Fig. 13(d), the thickness of the iron diffusion zone could be measured. The obtained thickness is about $d = 29.4$ μm. This thickness level is much low compared to the above estimation by Eq. (10). The reason behind this would be caused by the low iron content of 1.7% in the molten Al alloy (H-Fe). The chemical reaction between silicon nitride ceramic and iron was also studied experimentally by Heikinheimo et al.[37] An Fe(Si) solid solution was formed with the maximum silicon content of about 12 at.%, and no silicides were found at the metal ceramic interface. Fig. 14 displays the phase diagram of the Fe–Si system. The stable phases in the temperature around 973 K were mainly α-Fe, ε-FeSi and β-$FeSi_2$. Although the chemical reaction between silicon and iron is not clarified at the moment, that reaction could occur, as either Fe + Si → FeSi or Fe + 2Si → $FeSi_2$.[38] In the most stable silicide might be FeSi from the thermodynamic data available for Fe–Si diagram.[37] Oliveira et al. have also mentioned that the solid-state interaction between Si_3N_4 and steels can be appraised at high temperature

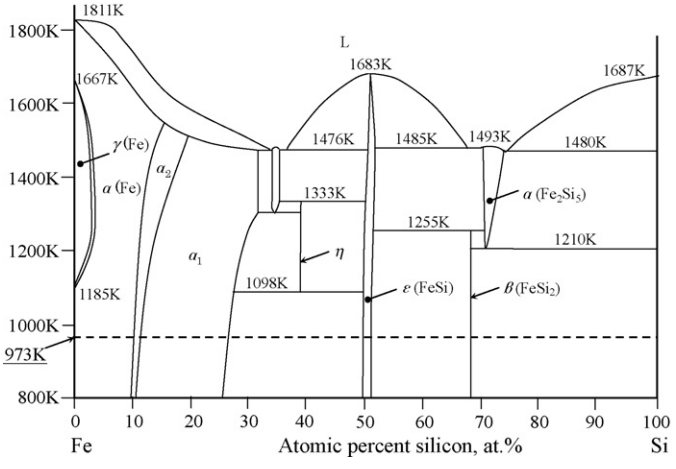

Fig. 14. Phase diagram of the Fe–Si system.

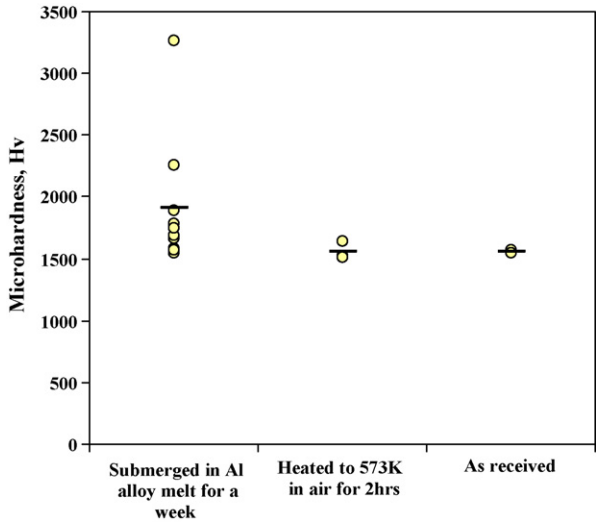

Fig. 15. Microhardness measurement of the Si_3N_4 ceramics under various conditions.

more than 1273 K.[3] From the above information, it could be considered that the iron diffusion and chemical reaction between Fe and Si_3N_4 would have occurred strongly, and this makes the change of the mechanical properties in the silicon nitride.

To understand the influence of the material properties on the mechanical strength of the silicon nitride ceramic, microhardness measurements of the Si_3N_4 specimen were carried out after scraping off the molten Al alloy on the ceramic with the results shown in Fig. 15. As can be seen, the microhardness of the samples at room temperature and 573 K were at the same level. This similar mechanical property is associated with similar bending strengths, as shown in Fig. 4. It can also be seen that the microhardness of Si_3N_4 submerged in molten aluminum alloys for a week is much higher, although the data are widely scattered. The high hardness of Si_3N_4 would be influenced by the iron content to the Si_3N_4 ceramic as mentioned above. Moreover, such an occurrence could cause the convex shape of the stress vs. deflection characteristic as seen in Fig. 4.

4. Conclusions

The mechanical and fatigue properties of Si_3N_4 ceramics have been studied experimentally. In this work, measurements have taken place at high temperatures in air and in molten aluminum alloys. From the present study, the following conclusions can be drawn:

(1) A clear reduction in the bending strength is observed when the samples are tested in the high air temperature and the molten aluminum alloys. The bending strengths for the sample tested at room temperature and at 573 K are almost same level, but this decreases slightly as the sample is heated to 1023 K. A considerable drop in the strength is obtained when the sample is immersed in the liquid aluminum alloys. Although the different strength, the slope of the stress vs. deflection relations is similarly obtained for all the samples.

(2) The reduction in the bending strength for the sample at 1023 K compared to the room temperature and at 573 K ones is influenced by oxidation of the Si_3N_4 ceramics. On the other hand, the low bending strength for the sample in the molten aluminum alloy is affected by the change in the material properties, where chemical reaction between iron and Si_3N_4 occurs.
(3) The profile of the stress–deflection curve in the beginning of the bending test in the liquid Al alloy shows convex although concave in the atmosphere ones. The change of bending properties of the samples tested in the molten Al alloy is influenced by the hardened ceramic (or brittleness) arising from the change of the material properties due to the chemical reaction by iron element. The mechanical strength of the Si_3N_4 in the liquid aluminum alloy is also sensitive to the amount of iron in the Al alloy, where the higher the iron content, the weaker the mechanical strength.
(4) The bending deflection level decreases with increase of the cycle number during the fatigue test in the molten aluminum alloys. The reason behind this is caused by the material hardening. Using the deflection value as parameter, the formula for the estimation of the damage variable to the final failure is proposed, and the damage variable increases with increasing cycle number. The variable of approximately 0.23 is the critical value to the fracture of this ceramic.

Acknowledgements

The authors would like to express the appreciation to Prof. F.J. Oliveira for helpful comments and suggestions on the manuscript. This work was supported by the grant (Young Scientists (B) 19760071, 2007) from the Japanese Government (Ministry of Education, Science, Sports and Culture). The authors would like to express their appreciation to Ms. Miho Sato at Akita Pref. Univ. and Mr. Makoto Kudo at Akita R&D Center for their technical support and useful advice.

References

1. Carrapichano, J. M., Gomes, J. R., Oliveira, F. J. and Silva, R. F., Si_3N_4 and Si_3N_4/SiC composite rings for dynamic sealing of circulating fluids. *Wear*, 2003, **255**, 695–698.
2. Kramer, B. M. and Judd, P. K., Computational design of wear coating. *J. Vac. Sci. Technol. A*, 1985, **3**, 2439–2444.
3. Oliveira, F. J., Silva, R. F. and Vieira, J. M., The reaction rate at Si_3N_4/steel interfaces as a function of sintering aids. *J. Eur. Ceram. Soc.*, 2002, **22**, 2561–2570.
4. Yang, J., Oliveira, F. J., Silva, R. F. and Ferreira, J. M., Pressureless sinterability of slip cast silicon nitride bodies prepared from coprecipitation-coated powders. *J. Eur. Ceram. Soc.*, 1999, **19**, 433–439.
5. Amaral, M., Oliveira, F. J., Belmonte, M., Fernandes, A. J. S., Costa, F. M. and Silva, R. F., Hot-filament chemical vapour deposition of nanodiamond on silicon nitride substrates. *Diamond Relat. Mater.*, 2004, **13**, 643–647.
6. Oliveira, F. J., Silva, R. F. and Vieira, J. M., Thermochemistry of contacts between silicon nitride ceramics and steels. *Acta Mater.*, 2000, **48**, 4659–4665.
7. Pal'guev, S. F., Lesunova, R. P., Burmakin, E. I. and Korovenkova, E. S., Electrochemical properties of nitride phases in the Si_3N_4–Ca_3N_2 and Si_3N_4–AlN–Ca_3N_2 systems. *Inorg. Mater.*, 2001, **37**, 684–687.
8. Babini, G. N., Bellosi, A. and Vincenzini, P., A diffusion model for the oxidation of hot pressed Si_3N_4–Y_2O_3–SiO_2 materials. *J. Mater. Sci.*, 1984, **19**, 1029–1042.
9. Bellosi, A., Vincenzini, P. and Babini, G. N., Stability of Si_3N_4–Al_2O_3–ZrO_2 composites in oxygen environments. *J. Mater. Sci.*, 1988, **23**, 2348–2354.
10. Vlasova, M. V., Bartnitskaya, T. S., Sukhikh, L. L., Krushinskaya, L. A., Tomila, T. V. and Artyuch, S. Y., Mechanism of Si_3N_4 nucleation during carbothermal reduction of silica. *J. Mater. Sci.*, 1995, **30**, 5263–5271.
11. Oliveira, F. J., Silva, R. F. and Vieira, J. M., Improved wear resistance of Si_3N_4 tool inserts by addition of Al_2O_3 platelets. *Tribol. Int.*, 2003, **36**, 57–60.
12. Okada, A., Automotive and industrial applications of structural ceramics in Japan. *J. Eur. Ceram. Soc.*, 2008, **28**, 1097–1104.
13. Fukushima, E., Method for producing Si_3N_4 ceramic and Si_3N_4 parts using in molten metals. Japan Patent, 1996-73286, 1993 [in Japanese].
14. Wang, L., Makhlouf, M. and Apelian, D., Aluminium die casting alloys: alloy composition, microstructure, and properties–performance relationships. *Int. Mater. Rev.*, 1995, **40**, 221–238.
15. Choi, J. C., Kwon, T. H., Park, J. H., Kim, J. H. and Kim, C. H., A study on development of a die design system for diecasting. *Int. J. Adv. Manuf. Technol.*, 2002, **20**, 1–8.
16. Ueki, S., Hot-chamber diecast machine for molten metals. Japan Patent, 2004-141965, 2004 [in Japanese].
17. Nogami, S. and Yashiro, T., Diecasting shot-sleeve. Japan Patent, 2004-34055, 2004 [in Japanese].
18. Okayasu, M., Hitomi, M. and Yamazaki, H., Hot chamber diecasting technology with a Si_3N_4 Ceramic for injection system: application to aluminum alloy components. *Int. J. Cast. Metal. Res.*, 2008, **21**, 339–348.
19. Kanazawa, K. and Okayasu, M., Effect of microstructure on mechanical properties and fracture toughness of aluminum alloy die castings. *Trans. Jpn. Soc. Mech. Eng.*, 1998, **64**, 1956–1963 [in Japanese].
20. Okayasu, M., Nishi, N. and Kanazawa, K., Effects of silicon contents on tensile properties of Al–Si–Cu alloy die castings. *J. Jpn. Foundry Eng. Soc.*, 1998, **70**, 266–272 [in Japanese].
21. Jung, Y. G., Choi, I. H. and Paik, U., Polymer absorption behavior following SiO_2 formation onto Si_3N_4 particle surface for in situ Si_3N_4/SiC nano-composite using polymer precursor. *J. Mater. Sci. Lett.*, 2000, **19**, 2113–2116.
22. Garshin, A. P. and Shvaikovskii, V. E. S., Studying the mechanism of the interaction between silicon nitride, oxygen, and nitrogen in heating and the processes of defect formation in Si_3N_4–gas systems. *Refract. Ind. Ceram.*, 1998, **39**, 314–318.
23. Babini, G. N., Bellosi, A. and Vincenzini, P., Oxidation of silicon nitride hot pressed with Y_2O_3 + MgO. *J. Mater. Sci.*, 1983, **18**, 231–244.
24. Kitayama, M., Hirao, K., Tsuge, A., Watari, K., Toriyama, M. and Kanzaki, S., Thermal conductivity of β-Si_3N_4: effect of lattice oxygen. *J. Am. Ceram. Soc.*, 2000, **83**, 1985–1992.
25. Okayasu, M., Ohtake, M., Bitoh, T. and Mizuno, M., Temperature dependence of the fatigue and mechanical properties of PZT ceramics. *Int. J. Fatigue*; submitted for publication.
26. Yuan, G. L., Liu, J. M., Wang, Y. P., Wu, D., Zhang, S. T., Shao, Q. Y. *et al.*, Temperature-dependent fatigue behaviors of ferroelectric ABO_3-type and layered perovskite oxide thin films. *Appl. Phys. Lett.*, 2004, **84**, 3352–3354.
27. Kitazumi, J., Taniguchi, Y., Hoshide, T. and Yamada, T., Characteristics of strength and their relations to flaw size distribution in several ceramic materials (Part 1: static strength). *Jpn. Soc. Mater. Sci.*, 1989, **38**, 24–30.
28. Wang, C., Fang, Q. F., Shi, Y. and Zhu, Z. G., Internal friction study on oxygen vacancies and domain walls in Pb(Zr, Ti)O_3 ceramics. *Mater. Res. Bull.*, 2001, **36**, 2657–2665.
29. Dusza, J., Sajgalik, P., Steen, M. and Semerad, E., Low-cycle strength under step loading of a Si_3N_4 + SiC nanocomposite at 1350 °C. *J. Mater. Sci.*, 2001, **36**, 4469–4477.
30. Pushpalal, G. K. D., Fracture behavior of calcium aluminate–phenol resin composite. *J. Mater. Sci.*, 2000, **35**, 981–987.
31. Yao, F., Ando, K., Chu, M. C. and Sato, S., Static and cyclic fatigue behaviour of crack-healed Si_3N_4/SiC composite ceramics. *J. Eur. Ceram. Soc.*, 2001, **21**, 991–997.

32. Qiao, G. J., Hongjie, W. and Zhihao, J., Comparison between fatigue behavior of some ceramics: a new concept of intrinsic stress-corrosion exponent n_0. *Int. J. Fatigue*, 2002, **24**, 499–508.
33. Okayasu, M., Aoki, S. and Mizuno, M., Effects of silver-based metal electroplate on fatigue properties of PZT ceramics. *Int. J. Fatigue*, 2008, **30**, 1115–1124.
34. Sonsino, C. M., Fatigue design of structural ceramic parts by the example of automotive intake and exhaust values. *Int. J. Fatigue*, 2003, **25**, 107–116.
35. Lemaitre, J., *A course on damage mechanics* (*2nd edition*). Springer, New York, 1996, pp. 21–37.
36. Oliveira, F. J., Silva, R. F., Ferreira, J. M. and Vieira, J. M., Colloidal processing and sintering behaviour of silicon nitride composites with nanosized alumina. *Key Eng. Mater.*, 1997, **132–136**, 1989–1992.
37. Heikinheimo, E., Isomaki, I., Kodentsov, A. A. and Loo, F. J. J. V., Chemical interaction between Fe and silicon nitride ceramic. *J. Eur. Ceram. Soc.*, 1997, **17**, 25–31.
38. Yamauchi, I., Suganuma, A., Okamoto, T. and Ohnaka, I., Effect of copper addition on the β-phase formation rate in $FeSi_2$ thermoelectric materials. *J. Mater. Sci.*, 1997, **32**, 4603–4611.